Kristofer K. Westbrook
Department of Mechanical Engineering,
University of Colorado,
Boulder, CO 80309

Vikas Parakh
Department of Biomedical and Chemical Engineering,
Syracuse University,
Syracuse, NY 13244

Taekwoong Chung
Department of Macromolecular Science and Engineering,
Case Western Reserve University,
Cleveland, OH 44106

Patrick T. Mather
Department of Biomedical and Chemical Engineering,
Syracuse University,
Syracuse, NY 13244

Logan C. Wan
Fairview High School,
Boulder, CO 80305

Martin L. Dunn

H. Jerry Qi[1]

Department of Mechanical Engineering,
University of Colorado,
Boulder, CO 80309

Constitutive Modeling of Shape Memory Effects in Semicrystalline Polymers With Stretch Induced Crystallization

*Polymers can demonstrate shape memory (SM) effects by being temporarily fixed in a nonequilibrium shape and then recover their permanent shape when exposed to heat, light, or other external stimuli. Many previously developed shape memory polymers (SMPs) use the dramatic molecular chain mobility change around the glass transition temperature T_g to realize the SM effect. In these materials, the temporary shape cannot be repeated unless it is reprogramed, and therefore the SM effect is one way. Recently, a semicrystalline SMP, which can demonstrate both one- and two-way SM effects, was developed by one of our groups (Chung, T., Rorno-Uribe, A., and Mather, P. T., 2008, "Two-Way Reversible Shape Memory in a Semicrystalline Network," Macromolecules, **41**(1), pp. 184–192). The main mechanism of the observed SM effects is due to stretch induced crystallization. This paper develops a one-dimensional constitutive model to describe the SM effect due to stretch induced crystallization. The model accurately describes the complex thermomechanical SM effect and can be used for the future development of three-dimensional constitutive models.* [DOI: 10.1115/1.4001964]

Keywords: shape memory polymers, soft active materials, constitutive models

1 Introduction

Shape memory polymers (SMPs) are a unique class of soft, active materials that can "memorize" their permanent (equilibrium) shape, be temporarily fixed in nonequilibrium shapes, and recover their permanent shape when exposed to heat, light, or other external stimuli. One advantage of SMPs over other shape memory (SM) materials is their ability to recover significantly larger shape changes. For example, as reported by Lendlein and Kelch [1], SMPs can recover an elongation at least as large as 150%, which is significantly larger than 8%, the largest shape recovery observed in shape memory alloys. This capability of large programmable shape change makes SMPs attractive in many applications, such as morphing structures and biomedical devices. Many previously developed SMPs use the dramatic molecular chain mobility change around the glass transition temperature T_g to realize the shape memory effect [1–3]. Briefly, a typical shape memory cycle is as follows. A SMP is isothermally predeformed (or programed) from an initial shape to a deformed shape (temporary shape) by applying a mechanical load at a temperature $T_H(T_H > T_g)$. The material will maintain its deformed shape after subsequently lowering the temperature to $T_L(T_L < T_g)$ and removing the external load. The SMP can largely maintain this shape as long as the temperature does not change. The SM effect is activated by raising the temperature to $T_D(T_D > T_g)$, where the initial shape is recovered under the driving force of entropic elasticity associated with the conformational entropy of the polymer network chains. In these SMPs, after the deployment, the SMP cannot achieve the temporary shape again by heating or cooling unless an external load is applied to deform the material. Therefore, such SMPs are termed "one-way" SMPs. Although the one-way shape memory (1W-SM) effect can meet the requirements for some applications where only a single deployment is required, it is highly desirable to develop a material that can demonstrate large "two-way" (2W) SM effects. For 1W-SMP to achieve a 2W-SM effect, a repeated loading is necessary.

Recently, a novel SMP that demonstrates 1W-SM [4] was also found to exhibit a significant 2W-SM effect [5]. After initially stretching the material at a high temperature (70°C), cooling the material from 70°C to 15°C under a tensile load induces a significant elongation. A subsequent heating back to 70°C reverses this elongation (the sample contracts), yielding a net 2W-SM effect. This SMP can also demonstrate the 1W-SM effect by removing the external load at the low temperature. The underlying mechanism responsible for these 2W- and 1W-SM effects is the stretch induced crystallization (SIC), which can cause stress relaxation under constant stretch. The promise of this material is due to the existence of the large 2W-SM effect. For example, as demonstrated in Ref. [5], up to 100% reversible stretch can be observed.

Although the SM effects have been realized in polymer physics a few decades ago, constitutive modeling of shape memory poly-

[1]Corresponding author.

Contributed by the Materials Division of ASME for publication in the JOURNAL OF ENGINEERING MATERIALS AND TECHNOLOGY. Manuscript received August 30, 2009; final manuscript received April 18, 2010; published online September 29, 2010. Assoc. Editor: Assimina Pelegri.

mers has been developed only recently, largely motivated by the recent developments of SMPs with very well defined shape control and the need for developing predictive analysis and design tools. Liu et al. [6] developed a 1D constitutive model where the 1W-SM effect is achieved by defining a storage deformation. In Liu et al. [6], a SMP is considered to consist of two phases, a rubbery phase and a glassy phase. During cooling of the material, some of the deformation in the rubbery phase is stored through an explicitly defined storage deformation. Based on Liu's phase concept and storage deformation, Chen and Lagoudas [7,8] extended Liu's model to a three-dimensional (3D) one. Recently, Qi et al. [2] developed a 3D finite deformation constitutive model for thermomechanical behaviors of SMPs without using a storage deformation. In Qi et al. [2], the model is based on the evolution of the deformation energy from an entropy dominated state to an enthalpy dominated state, which was modeled as a co-existence of two phases, one dominated by entropic energy and one dominated by the enthalpic energy. As the temperature is lowered, a new phase will be generated. The SM effect can be captured by allowing the newly formed phase to refer to the intermediate configuration or the current (deformed) configuration as its reference (undeformed) configuration. This implies that the newly formed phase is *undeformed* immediately upon its formation. Using this concept of an intermediate reference state, the SM effect can be effectively captured. A similar concept has also been forwarded by Rao and co-workers for crystallizable polymers [9,10]. For amorphous polymers, a different approach is called for and involves consideration of the dramatic change in viscosity in the material when the temperature traverses the glass transition temperature, as shown in Nguyen et al. [3]. On the other hand, for semicrystalline polymers, the phase evolution approach does represent the physical phenomena at work during deformation. In addition, it recently has been shown by the authors that such a modeling scheme can also be applied to other active polymers, such as photo-activated polymers, where new cross-links can be cleaved and reformed when irradiated by light with a certain wavelength [11].

In this paper, a constitutive model based on the concept of phase evolution is developed to quantitatively capture both 1W- and 2W-SM effects demonstrated in the semicrystalline polymers exhibiting SIC. The paper is arranged in the following manner: In Sec. 2, we describe briefly the material and experimental results that demonstrate the 1W- and 2W-SM effects. In Sec. 3, a general 1D constitutive model for finite deformation with evolving phases is presented in detail; the model is then used to consider both 1W- and 2W-SM behaviors due to SIC. In Sec. 4, results from the model are compared with those from the experiments. The effects of thermal rates to the SM effects are then investigated using this model.

2 Experiments

2.1 Materials. Samples were prepared using a procedure modified from prior work [4,5]. Poly(cyclooctene) (PCO) (Evonik-Degussa Corporation, Vestenamer 8012) with a trans content of 80% and dicumyl peroxide (DCP) (>98% purity, Aldrich) were used as received. All specimens were prepared using a Rancastle single screw Microtruder (RCP 0625) with a screw diameter of 15.875 mm and a working L/D ratio of 24:1 and a Carver press (model C). The Microtruder temperature was set at 70°C, 75°C, and 80°C for the feed, melting, and metering zones, respectively, and the die temperature was set to 80°C. The dried PCO pellets were then fed into the feed chamber and mixed with 2 wt % DCP based on the weight of PCO pellets to obtain the desirable composition in the final products at a rotation speed of 50 rpm. Such a process is capable of melting the polymer and uniformly dispersing the peroxide without inducing significant cross-linking. The mixture was then extruded from the microtruder and cut into small pellets and re-extruded to ensure homogeneous mixing. The final extrudates were cooled to room temperature. After adding into a spacer frame made of Teflon (thickness: 0.80 mm), the extrudate was pressed between two hot plates preheated to 180°C and then cured for 30 min under a load of ~4.45 kN which assured a good seal at the Teflon spacer. The fully cured samples were cooled to room temperature. The DCP content varied from 1 wt % to 2 wt % based on the weight of PCO. Only experimental results for PCO with 2 wt % of DCP are presented and used in this paper for the purpose of modeling; experimental results for similarly cross-linked PCO with other DCP weight contents can be found in Chung et al. [5].

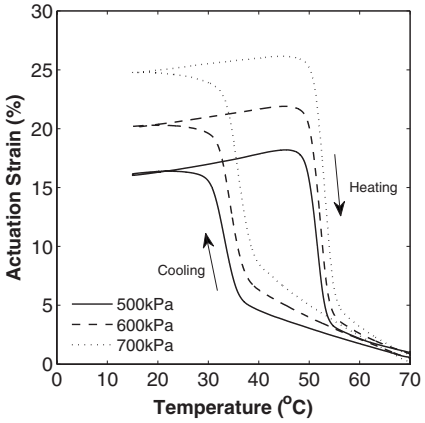

Fig. 1 Two-way shape memory effects demonstrated by the PCO material under different stresses

2.2 Thermomechanical Experiments. An MTS Universal Materials Testing Machine (Model Insight 10) was used to explore and analyze both 1W-SM and 2W-SM behaviors. This machine is equipped with a customized Thermcraft thermal chamber (Model LBO) using a temperature controller (Model Euro 2404) and an EIR laser extensometer (Model LE-05) for displacement/strain measurements. Samples were cut into rectangular strips with nominal dimensions of $0.8 \times 3.4 \times 30$ mm^3. In individual tests, the sample was placed in tension between a fixed upper stainless steel grip and a lower clamp for applying weights. A 1W-SM behavior was characterized using a four-step process. (1) *Deformation*: The PCO strip was elongated by attaching the applied load at $T_H(T_H > T_f)$, where T_f is the fusion temperature. (2) *Fixing*: The sample was then cooled at 2°C/min to a low temperature $T_L(T_L < T_m)$, where T_m was the melting temperature. (3) *Unloading*: The load was removed. (4) *Recovery*: The heat induced recovery toward the original length was examined by heating to T_H at a rate of 2°C/min.

In contrast, the 2W-SM cycle was conducted with the following three-step process. (1) *Deformation*: The sample was instantaneously stretched at $T_H(T_H > T_m)$. (2) *Cooling*: The deformed and loaded sample was then cooled to $T_L(T_L < T_m)$ at a rate of 2°C/min. (3) *Heating*: After being held for 10 min at T_L, the sample was then heated to T_H at a rate of 2°C/min. Characteristics of the 2W-SM behavior include the actuation strain $R_{act}(\sigma)$ defined as follows [5]:

$$R_{act}(\sigma) = \frac{L - L_{high}}{L_{high}} = \lambda_{act} - 1 \tag{1}$$

where L_{high} is the length of the sample at T_H, L is the length as the temperature varies, and λ_{act} is the actuation stretch.

2.3 Experimental Results

2.3.1 Two-Way Shape Memory Effect. Figure 1 shows the 2W-SM effects under different imposed stresses with $T_H = 70°C$ and $T_L = 15°C$. At T_H, the samples were preloaded to different stresses instantaneously. Decreasing the temperature induced an

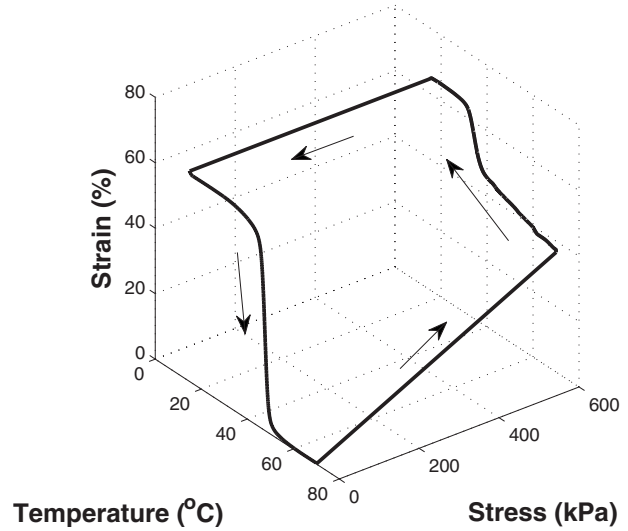

Fig. 2 One-way SM effect demonstrated by PCO under 600 kPa stress

actuation strain. Figure 1 shows three distinct regions during cooling: At the temperature above ~35°C (first region), actuation strain increases almost linearly with a relatively small slope that is dependent on the imposed stress; after the temperature is lower than ~35°C (the second region), the actuation strain increases with a relatively large slope; finally, the actuation strain saturates to a value that depends on the imposed stress. Reheating the sample recovers the original shape, which also shows three distinct regions. At the temperature lower than ~50°C (first region), the actuation further increases slightly; after the temperature traverses ~50°C (second region), the actuation strain decreases dramatically; finally, after the temperature is above ~55°C, the actuation strain decreases at a relatively small slope similar to that of cooling first region's slope. In addition to the three distinct regions during actuation and recover, two salient features can also be observed: First, the actuation strain strongly depends on the imposed stress. At the stresses of 500 kPa, 600 kPa, and 700 kPa, the actuation strains immediately after cooling are 16%, 20%, and 25%, respectively. Second, the actuation-recovery cycle shows a large hysteresis loop. In the experimental results shown in Fig. 1, the gap (hysteresis) between the cooling and heating curves is ~15°C.

2.3.2 One-Way Shape Memory Effect. The PCO material can also demonstrate the 1W-SM effect if the external load is removed after lowering down the temperature, as presented in Fig. 2. Specifically, at T_H, the sample is stretched by ~30% to reach a stress level of 500 kPa. Subsequently lowering the temperature, while maintaining the external load, induces actuation strain similar to that observed in the first half cycle of the 2W-SM effect shown in Fig. 1. At T_L, removal of the load causes a small contraction of the sample, while most of the strain is retained. Finally, increasing the temperature recovers the material to its original length. Note that the difference in the 1W-SM effects between the one in Fig. 2 and the one presented in previous studies [2] is that in Fig. 2 an external force was maintained during cooling, which induced further deformation, whereas in the previous work the compressive displacement was maintained, which diminished the force.

3 Constitutive Model

As introduced above, the observed 1W-SM and 2W-SM effects in the PCO material are due to SIC, which was experimentally verified by using wide angle X-ray scattering (WAXS) [5]. It is well known that SIC in rubbery materials can relax the stress when the material is cooled at constant deformation. This is because the intermolecular noncovalent interactions formed during SIC stores deformation. From a mechanics point of view, this storage mechanism can be understood as the reference (or undeformed) configuration for the newly formed SIC phases being the current configuration upon which they are formed. Such a concept was proposed to capture the shape memory behaviors of thermally induced SMPs and has been recently used to model photoactivated polymers [2,9]. In these previous studies, it was assumed that no significant deformation of the material occurs during the formation of the new phase. In the following, we generalize this theory under general loading conditions and then apply this generalized theory to model the observed and 1W- and 2W-SM effects.

3.1 Generalized 1D Theory. Here, we assume that the material is a mixture of a rubbery phase and a SIC phase. The volume fraction of each phase depends on the instantaneous temperature, deformation, and corresponding rate and history. To emphasize the mechanics aspect of the model, we ignore thermal contraction/expansion in the general theory. Thermal strain will be included when we consider the shape memory effect. In addition, we consider a relatively simple case where the nominal stress of the rubbery phase and the SIC phase are defined as

$$\sigma_r = \frac{\partial W_r(\lambda)}{\partial \lambda} \quad \text{and} \quad \sigma_{SIC} = \frac{\partial W_{SIC}(\lambda)}{\partial \lambda} \tag{2}$$

where W_r and σ_r are the strain energy function and stress for the rubbery phase and W_{SIC} and σ_{SIC} are the strain energy function and stress for the SIC phase. In the following discussion, the subscripts refer to the number of the SIC phase formed and the superscripts refer to the number of the time increment.

At time $t=0$ and temperature $T=T^0$, stretching the material by λ_0^0 induces a stress σ_{total}^0. For the sake of simplicity, we assume that the material consists of 100% rubbery phase at $t=0$. Therefore,

$$\sigma_{total}^0 = \sigma_r(\lambda_0^0) \tag{3}$$

At time $t=\Delta t$, a small volume fraction Δf_1 of SIC phase forms. One important assumption is that this newly formed SIC phase carries no deformation immediately upon its formation. Then, in order to satisfy the boundary conditions, the material will deform and introduce a small deformation increment $\Delta\lambda^1$. This assumption is consistent with the previous discussion that the SIC phase will relax the stress in some rubbers. In addition, such an assumption has been used by us and others to consider the 1W-SM effect [2,9,10]. The deformations in the rubbery phase and the new SIC phase, respectively, become

$$\lambda_0^1 = \Delta\lambda^1\lambda_0^0 \quad \text{and} \quad \lambda_1^1 = \Delta\lambda^1 \tag{4}$$

where λ_0^1 is the stretch in the initial rubbery phase (denoted by subscript 0) at the first time increment (denoted by superscript 1) and λ_1^1 is the stretch at the first time increment (denoted by superscript 1) in the SIC phase formed at the first time increment (denoted by subscript 1). The total stress at time $t=\Delta t$ becomes

$$\sigma_{total}^1 = [1-\Delta f_1]\sigma_r(\lambda_0^1) + \Delta f_1 \sigma_{SIC}(\lambda_1^1) \tag{5}$$

At time $t=n\Delta t$, there are $n+1$ replicates of phases, where n replicates are SIC phases formed at previous n time increments. The deformations in the rubbery phase ($i=0$) and the individual SIC phases ($1\le i\le n$) are

$$\lambda_0^n = \left[\prod_{k=1}^{n}\Delta\lambda^k\right]\lambda_0^0 \quad \text{and} \quad \lambda_i^n = \prod_{k=i}^{n}\Delta\lambda^k \tag{6}$$

where $\Delta\lambda^i$ is the new deformation induced at the ith time increment, λ_i^n is the total deformation in the ith replicate of the SIC phase (subscript, the phase formed at the ith time increment) at the nth time increment (superscript), and λ_0^n is the total deformation in the initial (rubbery) phase at the nth time increment (superscript).

Note a SIC phase formed at the ith time increment deforms at time increments thereafter, $1 \le i \le n$. The total stress at $t=n\Delta t$ is

$$\sigma_{\text{total}}^{n} = \left[1 - \sum_{k=1}^{n} \Delta f_k\right] \sigma_{\text{r}}(\lambda_0^n) + \sum_{k=1}^{n} [\Delta f_k \sigma_{\text{SIC}}(\lambda_k^n)] \tag{7a}$$

An integral formation of Eq. (7*a*) is

$$\sigma_{\text{total}} = \left[1 - \int_0^t \dot{f} ds\right] \sigma_{\text{r}}(\lambda(t)) + \int_0^t [\dot{f} \sigma_{\text{SIC}}(\lambda(t)\lambda^{-1}(s)) ds] \tag{7b}$$

Equations (6), (7*a*), and (7*b*) state the following:

(1) The ith phase only carries deformation after its formation; i.e., the ith replicate of the SIC phase uses the configuration at its creation as its reference (undeformed) configuration.
(2) The deformation increment in each time increment applies equally to each phase.

In the above equations, Δf_i and $\Delta\lambda^i$ $(1 \le i \le n)$ are internal variables. The number of internal variables is thus twice the total number of time increments. In a general 3D finite deformation, finite element implementation, this method is prohibitively expensive for two reasons. First, it will require a very large amount of system memory to store these internal variables at every integration point. Second, in Eq. (7), the stress for each phase changes in every time increment. However, for the 1D case considered in this paper, Eq. (7) can be greatly simplified when the Hencky strain is used to define the constitutive behaviors. Recently, a computational efficient scheme to address these issues is developed in 1D [12]. The 3D implementation of this scheme is conducted by the authors and will be reported in the future.

3.2 Shape Memory Effect Due to SIC. In the following, we develop a 1D model for the SM effects due to SIC based on the generalized model described above. Since the material developed here works at temperatures well above its T_g, we adopt a simple large deformation elasticity model by assuming that both the rubbery phase and the SIC phase follow the similar form of stress-strain behavior,

$$\sigma_{\text{r}}(\lambda_0^n) = NkT \ln \lambda_0^{n,M} \tag{8a}$$

$$\sigma_{\text{SIC}}(\lambda_i^n) = \mu \ln \lambda_i^{n,M} \tag{8b}$$

where $\lambda_0^{n,M}$ and $\lambda_i^{n,M}$ are the stretch ratios due to only mechanical deformation in the initial rubbery phase and the ith $(1 \le i \le n)$ replicate of the SIC phase at the nth time increment, N is the cross-link density of the polymer, k is Boltzmann's constant, and μ is the modulus of the SIC phase. Equation (8*a*) states that the modulus of the rubbery phase depends on the temperature, which is a well known behavior for rubbers or elastomers whose stress-strain behavior is dominated by the variation in entropy. Here, Hencky strains are used as they conveniently convert the multiplicative operation of stretches into additive strains, which greatly simplifies the work of tracking deformation in individual SIC phases.

At time $t=0$, the temperature is T^0, and the stretch due to a stress σ is

$$\lambda_0^0 = \exp\left(\frac{\sigma}{NkT^0}\right) \tag{9}$$

At time $t=\Delta t$, the temperature changes by ΔT^1 and a small volume fraction Δf_1 of SIC phase forms, introducing a small deformation $\Delta\lambda^1$. The deformations in the rubbery phase and the new SIC phase, respectively, become

$$\lambda_0^1 = \Delta\lambda^1 \lambda_0^0 \text{ and } \lambda_1^1 = \Delta\lambda^1 \tag{10}$$

Here, $\Delta\lambda_1$ has contributions from both mechanical and thermal deformations, i.e.,

$$\Delta\lambda^1 = \Delta\lambda^{1,T}\Delta\lambda^{1,M} \text{ and } \Delta\lambda^{1,T} = 1 + \alpha(T)\Delta T^1 \tag{11}$$

where $\Delta\lambda^{1,T}$ is the stretch due to thermal expansion, $\Delta\lambda^{1,M}$ is the new mechanical stretch, α is the temperature dependent linear coefficient of thermal expansion (CTE), and ΔT^1 is the temperature increment in the first time increment. The mechanical stretches, which give rise to the stress, in the rubbery phase and the new SIC phase, respectively, are

$$\lambda_0^{1,M} = \Delta\lambda^{1,M}\lambda_0^0 \text{ and } \lambda_1^{1,M} = \Delta\lambda^{1,M} \tag{12}$$

At $t=n\Delta t$, a small volume fraction Δf_n of the SIC phase forms, introducing a small new deformation $\Delta\lambda^n$. The respective deformations in the rubbery phase and the ith SIC phase are

$$\lambda_0^n = \left(\prod_{k=1}^{n} \Delta\lambda^k\right)\lambda_0^0 \text{ and } \lambda_i^n = \prod_{k=i}^{n} \Delta\lambda^k \tag{13}$$

The $\Delta\lambda^k$ has contributions from both mechanical $(\Delta\lambda^{k,M})$ and thermal deformations $(\Delta\lambda^{k,T})$, i.e.,

$$\Delta\lambda^k = \Delta\lambda^{k,T}\Delta\lambda^{k,M} \text{ and } \Delta\lambda^{k,T} = 1 + \alpha(T)\Delta T^k \tag{14}$$

where ΔT^k is the temperature increment in the kth time increment. The mechanical stretches in the rubbery phase and the ith replicate of the SIC phase are

$$\lambda_0^{n,M} = \left(\prod_{k=1}^{n} \Delta\lambda^{k,M}\right)\lambda_0^0 \text{ and } \lambda_i^{n,M} = \prod_{k=i}^{n} \Delta\lambda^{k,M} \tag{15}$$

The total thermal stretch is

$$\Delta\lambda_{\text{total}}^{T} = \prod_{k=1}^{n} \Delta\lambda^{k,T} \tag{16}$$

Note that the total stretch in the ith SIC phase λ_i^n is required to satisfy any geometrical constraints, whereas the total mechanical stretch in the ith SIC phase $\lambda_i^{n,M}$ gives rise to stress and is required to satisfy force balance.

3.2.1 One-Way Shape Memory Effect. For the 1W-SM effect described above, a constant nominal stress $\bar{\sigma}$ is applied to deform at a temperature T^0 and then fix the shape (cooling and mechanical unloading). For the case of using constant displacement to fix the shape, see the Appendix. The SM recovery effect is activated by increasing the temperature. In the initial deformation, the constant stress, $\bar{\sigma}$, causes a stretch of the material,

$$\lambda_0^0 = \exp\left(\frac{\bar{\sigma}}{NkT^0}\right) \tag{17}$$

At time $t=n\Delta t$, from Eqs. (7*a*), (8), and (15),

$$\bar{\sigma} = \left[1 - \sum_{k=1}^{n} \Delta f_k\right] NkT(n\Delta t)\left[\ln \lambda_0^0 + \sum_{k=1}^{n} \ln \Delta\lambda^{k,M}\right] + \mu\left[\sum_{i=1}^{n} \Delta f_i \left(\sum_{k=i}^{n} \ln \Delta\lambda^{k,M}\right)\right] \tag{18}$$

The increment of mechanical stretch can be solved as

$$\Delta\lambda^{n,M}=\exp\left\{\frac{\bar{\sigma}^n-\left(1-\sum_{k=1}^{n}\Delta f_k\right)NkT(n\Delta t)\left(\ln\lambda_0^0+\sum_{k=1}^{n-1}\ln\Delta\lambda^{k,M}\right)-\mu\left[\sum_{i=1}^{n}\Delta f_i\left(\sum_{k=i}^{n-1}\ln\Delta\lambda^{k,M}\right)\right]}{\left(1-\sum_{k=1}^{n}\Delta f_k\right)NkT(n\Delta t)+\mu\sum_{k=1}^{n}\Delta f_k}\right\} \tag{19}$$

The total increase in the stretch is given by Eq. (14). Because of the additive nature of the Hencky strain, the number of internal variables in Eq. (19) is reduced to 3, i.e.,

$$f_n=\sum_{k=1}^{n}\Delta f_k,\quad s_1^n=\sum_{k=1}^{n-1}\ln\Delta\lambda^{k,M},\ \text{and}\ s_2^n=\sum_{i=1}^{n}\Delta f_i\left(\sum_{k=i}^{n-1}\ln\Delta\lambda^{k,M}\right) \tag{20}$$

The variable s_2^n can be updated by

$$s_2^{n+1}=s_2^n+\Delta f_{n+1}\ln\Delta\lambda^{n+1,M} \tag{21}$$

During mechanical unloading, a mechanical deformation $\Delta\lambda_u$ is introduced, which gives rise to a zero total stress,

$$\left(1-\sum_{k=1}^{n_1}\Delta f_k\right)NkT_u\left(\ln\lambda_0^0+\sum_{k=1}^{n_1}\ln\Delta\lambda^{k,M}+\ln\Delta\lambda_u\right)+\mu\left[\sum_{i=1}^{n_1}\Delta f_i\left(\sum_{k=i}^{n_1}\ln\Delta\lambda^{k,M}+\ln\Delta\lambda_u\right)\right]=0 \tag{22}$$

where n_1 is the total number of increments during shape fixing and T_u is the temperature at which unloading occurs. Therefore,

$$\Delta\lambda_u=\exp\left\{-\frac{\left(1-\sum_{k=1}^{n_1}\Delta f_k\right)NkT_u\left(\ln\lambda_0^0+\sum_{k=1}^{n_1}\ln\Delta\lambda^{k,M}\right)-\mu\left[\sum_{i=1}^{n_1}\Delta f_i\left(\sum_{k=i}^{n_1}\ln\Delta\lambda^{k,M}\right)\right]}{\left(1-\sum_{k=1}^{n_1}\Delta f_k\right)NkT_u+\mu\sum_{k=1}^{n_1}\Delta f_k}\right\} \tag{23}$$

During reheating, a similar process, as described in Eq. (19), can be invoked but with $\bar{\sigma}=0$.

3.2.2 Two-Way Shape Memory Effect. For the 2W-SM effect, a constant stress is applied during the entire actuation and recovery cycle, and Eq. (19) can therefore be used for both cooling and reheating. The total change in the stretch ratio $\Delta\lambda$ becomes

$$\Delta\lambda=\prod_{i=1}^{n}\Delta\lambda^{i,M}\prod_{i=1}^{n}\Delta\lambda^{i,T} \tag{24}$$

3.3 Evolution Rule for SIC. The kinetics of the oriented crystallization process is generally described by Avrami's phase transition theory [13,14] modified by Gent [15] for SIC,

$$f(t)=f(\infty)\left[1-\exp\left(-\frac{k_c t^q}{f(\infty)}\right)\right] \tag{25}$$

where k_c is the crystallization rate constant and q is a constant related to the geometry of crystallinity. Gent suggested that $q=1$ for aciform crystal growth and $q=3$ for spherical crystal growth. Luch and Yeh confirmed that $q=1$ is the case when the stretching ratio is moderate [16]. In Eq. (25), temperature is not explicitly present due to the fact that most previous SIC studies used a quenched method where the temperature was constant. Here, based on the concept in Avrami's phase transition theory, we propose the following evolution rule for one-dimensional SIC.

Previous experimental results showed that crystallization only occurs after the temperature is lower than a temperature, called fusion temperature T_f. In addition, as shown in the experiments of PCO, there exists a critical stress/stretch, below which no SIC phase forms. Therefore, the fusion rate $\dot{f}_f$ is

$$\dot{f}_f=k_f(f_\infty-f)(T_f-T)(\lambda-\lambda_{crit})\quad \text{if}\ (T<T_f\ \text{and}\ \lambda>\lambda_{crit}) \tag{26}$$

where f is the volume fraction of the SIC phase, k_f is the fusion efficiency factor, and f_∞ is the volume fraction at time $t=\infty$. Similar to the fusion process, as the temperature increases, melting starts if the temperature is above a melting temperature T_m. Therefore, the melting rate $\dot{f}_m$ is

$$\dot{f}_m=k_m f(T-T_m)\quad \text{if}\ (T>T_m) \tag{27}$$

where k_m is the melting efficiency factor.

The total rate of SIC formation is

$$\dot{f}=\dot{f}_f-\dot{f}_m \tag{28}$$

In addition, the volume fraction of SIC should satisfy

$$0\le f\le f_\infty \tag{29}$$

3.4 CTE. Due to the differences in the macromolecular arrangements, the rubbery and SIC phases may have different CTEs. In addition, it is well known that SIC formation is accompanied by a volume change. Based on these two observations, an effective CTE at $t=n\Delta t$ can be calculated as

$$\alpha^n(T)=\left(1-\sum_{i=1}^{n}\Delta f_i\right)\alpha_a+\sum_{i=1}^{n}\Delta f_i\alpha_{SIC}+\alpha_{tran}\frac{\Delta f_i}{\Delta T^n} \tag{30}$$

where α_a is the CTE of the rubbery phase, α_{SIC} is the CTE of the SIC phase, and α_{tran} is the volume expansion ratio during phase transition from the rubbery phase to the SIC phase; ΔT^n is the temperature increment at the nth time increment.

4 Results

4.1 Two-Way Shape Memory Effect. The experimental results from the 2W-SM cycle with a 700 kPa imposed stress were

Table 1 Model parameters

Description	Parameter	Value
Shape memory effect due to SIC (Sec. 3.2)		
Polymer cross-linking density	Nk (Pa/K)	4.7×10^{3}
SIC phase modulus	μ (MPa)	16
Evolution rule for SIC Sec. 3.3		
Fusion temperature	T_{f} (°C)	42
Melting temperature	T_{m} (°C)	47
Volume fraction at time $t=\infty$	f_{∞}	0.8
Critical stretch for SIC phase	λ_{crit}	1.05
Fusion efficiency factor	k_f	1.0×10^{-3}
Melting efficiency factor	k_m	5.5×10^{-3}
Coefficient of thermal expansion Sec. 3.4		
Rubbery phase CTE	α_a ($^{\circ}\mathrm{C}^{-1}$)	1.0×10^{-4}
SIC phase CTE	α_{SIC} ($^{\circ}\mathrm{C}^{-1}$)	5.0×10^{-4}
Phase transition volume expansion ratio	α_{tran}	3.0×10^{-4}

used to fit the model parameters, which are listed in Table 1. These parameters were used for the rest of the simulations in this section. Figure 3(*a*) shows the model fit. It is noted that because the actuation strain is not very sensitive to the CTE, CTE parameters cannot be determined accurately from the actuation experiments. The excellent agreement between model simulation and experiment validates that the model captures the essential features demonstrated in the 2W-SM effect. The model simulation is able to predict the ~1% residual strain after heating the material to 70°C shown in the experiments.

The model also reveals the underlying physics for the 2W-SM behavior demonstrated by the material. During cooling (or actuation), the initial gradual increase in actuation strain before the fusion temperature ($T_{\mathrm{f}}=40^{\circ}\mathrm{C}$) is due to the temperature dependence of the modulus of entropic elasticity (Eq. (8*a*)). As the temperature decreases, according to Eq. (8*a*), the modulus of entropic elasticity decreases, which leads to an increase in the elongation in order to maintain the stress. After the temperature is decreased below the fusion temperature, SIC phases start to form. As described by Eq. (13), the fraction of the SIC phase formed at a later time carries a smaller deformation than the fraction of SIC formed at an earlier time. This results in a smaller effective deformation in the SIC phase than the mechanical actuation stretch. This can be illustrated by defining the effective deformation $\bar{\lambda}^{n,M}$ in the SIC phase,

$$\sigma_{\mathrm{SIC}}=\mu\left[\sum_{i=1}^{n}\Delta f_i\left(\sum_{k=i}^{n}\ln\Delta\lambda^{k,M}\right)\right]=\mu\left(\sum_{i=1}^{n}\Delta f_i\right)\ln\bar{\lambda}^{n,M} \tag{31}$$

From Eq. (31), we have

$$\bar{\lambda}^{n,M}=\exp\left\{\frac{\displaystyle\sum_{i=1}^{n}\left[\Delta f_i\left(\sum_{k=i}^{n}\ln\Delta\lambda^{k,M}\right)\right]}{\displaystyle\sum_{i=1}^{n}\Delta f_i}\right\} \tag{32}$$

Note that the mechanical actuation stretch is $\lambda_{\mathrm{act}}^{M}=\Pi_{k=1}^{n}\Delta\lambda^{k,M}$ from Eq. (32), $\bar{\lambda}^{n,M}<\lambda^{n,M}$. Figure 3(*b*) shows the comparison between the mechanical actuation stretch and the effective stretch in the SIC phase as a function of stress in the SIC phase. It is clear that the effective stretch in the SIC phase is much smaller than the mechanical actuation stretch.

From the above discussion, two strain actuation mechanisms become evident: The first one is due to the decrease in the modulus of entropic elasticity, and the second is due to the formation of the SIC phase. For temperatures above T_{f}, only the first mechanism functions, and at a temperature below T_{f}, both mechanisms function, with a decreasing contribution from the first mechanism as the volume fraction of the rubbery phase decreases. The contribution from the second mechanism also diminishes as the volume fraction of the SIC phase reaches its saturation value.

During reheating, the initial slight increase in actuation strain is due to the thermal expansion of the SIC phase. As the temperature increases above the melting temperature T_{m}, the SIC phase starts to melt, which results in the stored deformation in the SIC phase being released and a decrease in the actuation strain. After ~50°C, the SIC phase is almost completely melted, resulting in the recovery of actuation due to the first actuation mechanism.

The material parameters identified by fitting the 700 kPa curve were then used to predict actuations with stresses of 500 kPa and 600 kPa. Figure 4 shows the comparison between model predictions and experiments. The good agreement between the model predictions and the experiments verifies the model.

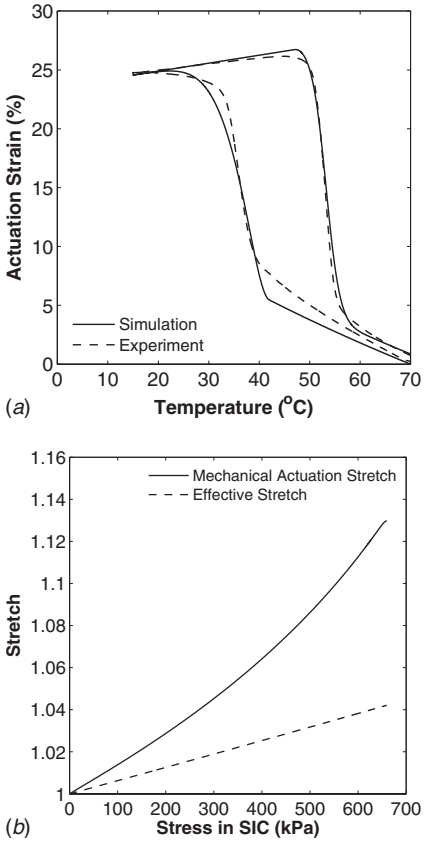

Fig. 3 (*a*) Model fit to the experimental result for the case of imposed stress 700 kPa. (*b*) Comparisons between mechanical actuation stretch and effective stretch in SIC.

4.2 One-Way Shape Memory Effect. Using parameters listed in Table 1, the 1W-SM effect is also simulated. The comparison between the model prediction and the experiment for the 600 kPa stress is shown in Fig. 5, which shows good agreement. Since material parameters are identified using the 2W-SM experimental result, this good agreement further justifies the model.

4.3 Effects of Heating/Cooling Rates. Since the formation of the SIC phase is a rate dependent process, the effects of heating and cooling rates on the 2W actuations were studied. Here, we use the same temperature rates for heating and cooling in one 2W-SM simulation. Figure 6(*a*) shows the 2W-SM effects at temperature rates (both heating and cooling) of 0.2°C/min, 2°C/min, and 20°C/min for a stress of 500 kPa. Similar results are expected for

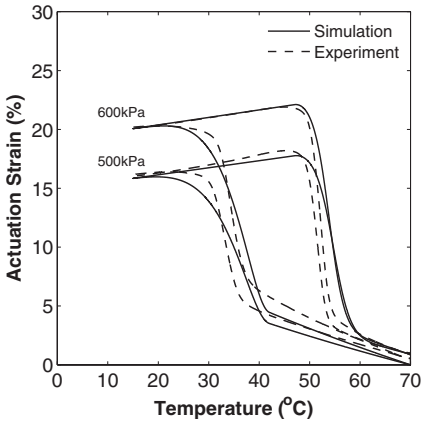

Fig. 4 Comparisons between model predictions and experimental results for the case of 500 kPa and 600 kPa imposed stresses

other applied stresses, though with quantitative differences. In these simulations, heating starts immediately after the temperature is cooled down to T_L from T_H. It is noticed that the maximum actuation strain is higher at 2°C/min than those at 0.2°C/min and 20°C/min. Figure 6(*b*) shows the dependence of the maximum actuation strains during the cooling-heating cycle and immediately after the cooling step versus cooling/heating rates. The latter presents a peak value of ~15.7% at a cooling/heating rate of ~0.002°C/min. Note the difference between the maximum actuation strains during cooling and heating and those immediately after the cooling. This difference is because the SIC phase may further develop even after cooling ends if the cooling rate is high. Figure 6(*c*) shows the evolution of the SIC phase volume fraction as a function of temperature at different cooling/heating rates. At a rate of 20°C/min, due to the high cooling rate, the SIC phase cannot reach its saturation value at a low temperature; actually, the SIC phase can still form during heating. The lack of a fully developed SIC phase results in the observed lower actuation strains. Alternatively, when the rate is relatively slow (0.2°C/min), the SIC phase reaches the saturation volume fraction in less than 10°C below the fusion temperature (T_f=40°C), resulting in a slightly lower actuation strain, as observed in Fig. 6(*a*). This is because in the case of the 2°C/min cooling rate, the rubbery

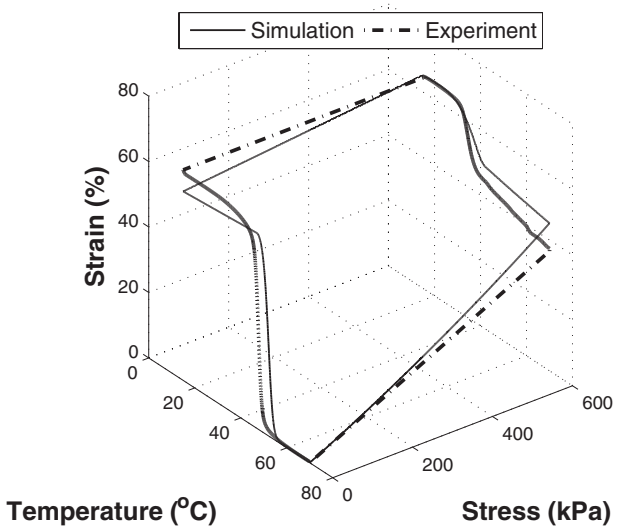

Fig. 5 Comparison between the model simulation and the experiment for the one-way SM effect under 600 kPa stress

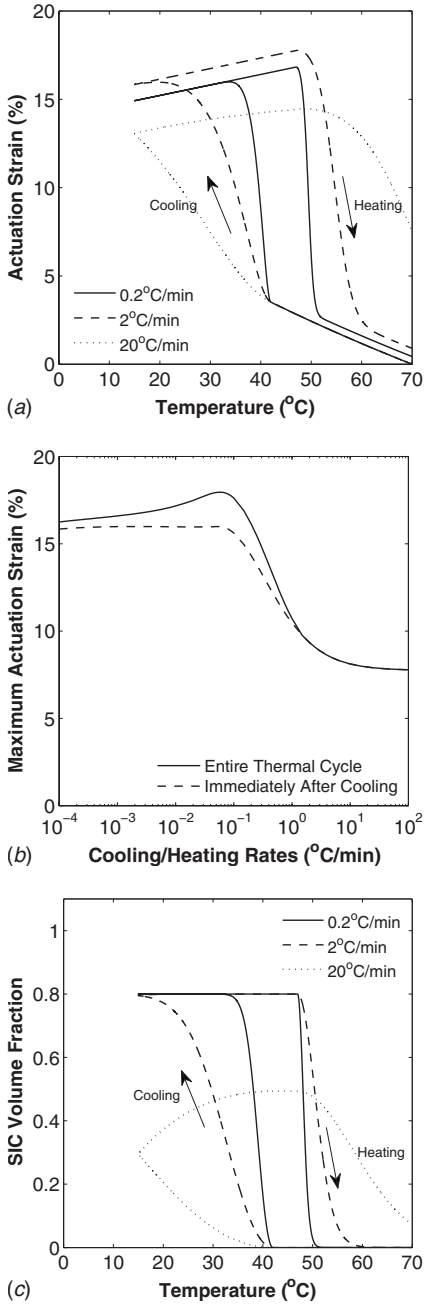

Fig. 6 Effects of temperature rates on the two-way SM effects under 500 kPa stress: (*a*) actuation strain, (*b*) actuation strain immediately after cooling, and (*c*) SIC volume fraction

phase volume fraction decreases relatively slowly; the presence of the rubbery phase can contribute to the actuation through the first actuation mechanism (decrease in modulus of entropic elasticity). When the cooling rate is slower, the contribution to the actuation strain by the first mechanism decreases quickly since the volume fraction of the rubber phase reaches its final value at a higher temperature.

In the above discussion, the dependence of actuation strain on the cooling/heating rates assumes that the material is heated immediately after cooling, which corresponds to the application with a continuous cyclic actuation. In some applications, the material is stored at a low temperature for a period of time before later actuation by heating. Here, the effect of cooling rates is investigated under the conditions where the sample is first cooled and then held at a low temperature (below T_f and T_m). Figure 7 shows the

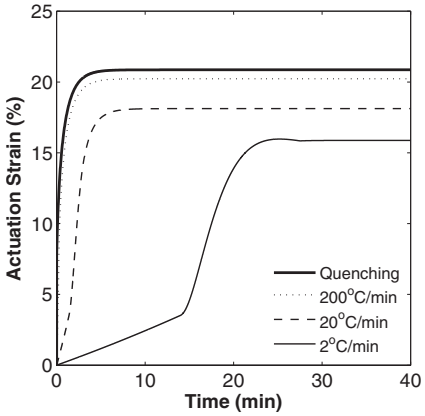

Fig. 7 Effects of temperature rates on the actuation strain for the case of cooling followed by holding the sample

evolution of the actuation strains as a function of time with different cooling rates. Figure 7 also shows the quenching case, simulated here by setting the cooling rate to $20{,}000\,^{\circ}\mathrm{C/min}$. It is seen that a faster cooling rate can generate a larger actuation strain. This is a result of the formation of the SIC phase that lags behind the temperature change at a faster cooling rate, which allows the rubbery phase to contribute to the actuation strain through the first strain actuation mechanism (the decrease in the modulus of entropic elasticity). In the quenching case, there is not enough time for the SIC phase to form upon reaching a low temperature, and therefore, the actuation from the rubbery phase is fully utilized. Hence, quenching corresponds to the maximum actuation strain that one can obtain.

5 Conclusions

This paper investigated and modeled the SM effects demonstrated by a semicrystalline polymer [5], in which the SM effect is due to the formation of SIC phases as the temperature decreases. Since the SIC formation is a rate dependent process, the deformation states within the individual SIC phases formed at different times are different. Based on this observation, a 1D constitutive model was developed. The model showed excellent agreement with diverse experimental results. The model was also used to explore the effects of temperature rates on the actuation strain in the 2W-SM actuation. Based on this validation, the model can be used in the future for mechanical design with such SMPs characterized by an underlying semicrystalline network structure. The proposed model is a 1D model. To expand this model into a 3D model, one critical step is to understand how SIC develops under multi-axial loading conditions and how the process of SIC formation influences the SM effect. These are currently being studied by the authors and will be reported in the future.

Acknowledgment

The authors gratefully acknowledge the support from an AFOSR grant (Grant No. FA9550-09-1-0195) to P.T.M., H.J.Q., and M.L.D., a NSF career award to H.J.Q. (Grant No. CMMI-0645219), and a NSF grant to P.T.M. (Grant No. DMR-0758631).

Appendix: One-Way SM Effect With Geometrical Constraints

As seen in Fig. 2, when a constant force is applied during shape fixing, additional deformation will be induced. In practice, displacement is typically fixed during shape fixing. As expected, mechanical stress will therefore vary during this process. Below, we present the stress variation during the shape fixing. Unloading and reheating follow the same rules described in Eqs. (22)–(24). During shape fixing, a constant strain is applied, i.e.,

$$\lambda_0^0 = \exp\left(\frac{\bar{\sigma}}{NkT^0}\right) = \bar{\lambda} \tag{A1}$$

At time $t=\Delta t$, from Eqs. (13)–(16),

$$\lambda_0^1 = \Delta\lambda^{1,T}\Delta\lambda^{1,M}\lambda_0^0 = \bar{\lambda} \tag{A2}$$

Combining Eqs. (A1) and (A2),

$$\Delta\lambda^{1,T}\Delta\lambda^{1,M} = 1 \tag{A3}$$

and the total stress is

$$\sigma^1 = (1-\Delta f_1)NkT(\Delta t)\ln(\Delta\lambda^{1,M}\bar{\lambda}) + \Delta f_1 \mu \ln \Delta\lambda^{1,M} \tag{A4}$$

At time $t=n\Delta t$, from Eqs. (13)–(16)

$$\lambda_0^n = \left(\prod_{k=1}^{n}\Delta\lambda_k^M \prod_{k=1}^{n}\Delta\lambda_k^T\right)\lambda_0^0 = \bar{\lambda} \tag{A5}$$

and therefore

$$\Delta\lambda_n^M = \left(\prod_{k=1}^{n-1}\Delta\lambda_k^M \prod_{k=1}^{n}\Delta\lambda_k^T\right)^{-1} \tag{A6}$$

The total stress becomes

$$\sigma^n = \left[1-\sum_{k=1}^{n}\Delta f_k\right]NkT(n\Delta t)\left(\bar{\lambda}\sum_{k=1}^{n}\ln\Delta\lambda^{k,M}\right) + \mu\left[\sum_{i=1}^{n}\Delta f_i\left(\sum_{k=i}^{n}\ln\Delta\lambda^{k,M}\right)\right] \tag{A7}$$

References

[1] Lendlein, A., and Kelch, S., 2002, "Shape-Memory Polymers," Angew. Chem., Int. Ed., **41**(12), pp. 2034–2057.
[2] Qi, H. J., Nguyen, T. D., Castro, F., Yakacki, C., and Shandas, R., 2008, "Finite Deformation Thermo-Mechanical Behavior of Thermally Induced Shape Memory Polymers," J. Mech. Phys. Solids, **56**, pp. 1730–1751.
[3] Nguyen, T. D., Qi, H. J., Castro, F., and Long, K. N., 2008, "A Thermoviscoelastic Model for Amorphous Shape Memory Polymers: Incorporating Structural and Stress Relaxation," J. Mech. Phys. Solids, **56**(9), pp. 2792–2814.
[4] Liu, C. D., Chun, S. B., Mather, P. T., Zheng, L., Haley, E. H., and Coughlin, E. B., 2002, "Chemically Cross-Linked Polycyclooctene: Synthesis, Characterization, And Shape Memory Behavior," Macromolecules, **35**(27), pp. 9868–9874.
[5] Chung, T., Rorno-Uribe, A., and Mather, P. T., 2008, "Two-Way Reversible Shape Memory in a Semicrystalline Network," Macromolecules, **41**(1), pp. 184–192.
[6] Liu, Y. P., Gall, K., Dunn, M. L., Greenberg, A. R., and Diani, J., 2006, "Thermomechanics of Shape Memory Polymers: Uniaxial Experiments and Constitutive Modeling," Int. J. Plast., **22**(2), pp. 279–313.
[7] Chen, Y. C., and Lagoudas, D. C., 2008, "A Constitutive Theory for Shape Memory Polymers. Part I: Large Deformations," J. Mech. Phys. Solids, **56**(5), pp. 1752–1765.
[8] Chen, Y. C., and Lagoudas, D. C., 2008, "A Constitutive Theory for Shape Memory Polymers. Part II: A Linearized Model for Small Deformations," J. Mech. Phys. Solids, **56**(5), pp. 1766–1778.
[9] Barot, G., and Rao, I. J., 2006, "Constitutive Modeling of the Mechanics Associated With Crystallizable Shape Memory Polymers," ZAMP, **57**(4), pp. 652–681.
[10] Barot, G., Rao, I. J., and Rajagopal, K. R., 2008, "A Thermodynamic Framework for the Modeling of Crystallizable Shape Memory Polymers," Int. J. Eng. Sci., **46**(4), pp. 325–351.
[11] Long, K. N., Scott, T. F., Qi, H. J., Bowman, C. N., and Dunn, M. L., 2009, "Photomechanics of Light-Activated Polymers," J. Mech. Phys. Solids, **57**(7), pp. 1103–1121.
[12] Long, K. N., Dunn, M. L., and Qi, H. J., 2010, "Mechanics of Soft Active Materials With Evolving Phases," Int. J. Plast., **26**(4), pp. 603-616.

[13] Avrami, M., 1939, "Kinetics of Phase Change. I General Theory," J. Chem. Phys., **7**(12), pp. 1103–1112.
[14] Avrami, M., 1941, "Granulation, Phase Change, and Microstructure Kinetics of Phase Change. III," J. Chem. Phys., **9**(2), pp. 177–184.
[15] Gent, A. N., 1954, "Crystallization and the Relaxation of Stress in Stretched Natural Rubber Vulcanizates," Trans. Faraday Soc., **50**(5), pp. 521–533.
[16] Luch, D., and Yeh, G. S. Y., 1973, "Strain-Induced Crystallization of Natural-Rubber.3. Re-Examination of Axial-Stress Changes During Oriented Crystallization of Natural-Rubber Vulcanizates," J. Polym. Sci., Part B: Polym. Phys., **11**(3), pp. 467–486.